Studying Criticality and Excitations of One Dimensional Systems by Time Matrix Product States

Emanuele Tirrito,[1] Luca Tagliacozzo,[2] Maciej Lewenstein,[1,3] and Shi-Ju Ran[4,1,*]

[1]*ICFO-Institut de Ciencies Fotoniques, The Barcelona Institute of Science and Technology, 08860 Castelldefels (Barcelona), Spain*
[2]*Department of Physics and SUPA, University of Strathclyde, Glasgow G4 0NG, United Kingdom*
[3]*ICREA-Institució Catalana de Recerca i Estudis Avançats, Lluis Companys 23, 08010 Barcelona, Spain*
[4]*Department of Physics, Capital Normal University, Beijing 100048, China*

In this work, we propose to access the information of criticality and excitations of one-dimensional quantum systems by a matrix product state (MPS) defined in the (imaginary) time direction. This state, dubbed as time MPS (tMPS), is a boundary state of tensor network (TN) that represents the ground-state simulation after Trotter-Suzuki decomposition. We show that the tMPS exhibits the structure of the continuous MPS originally proposed for the field theories. The information of excitations, e.g., dynamic correlation length and energy gap, can be accurately calculated from the tMPS. The non-universal renormalization of velocity of the excitations is given by a ratio between the correlations of the ground state and the tMPS. When the system is at the quantum critical point, the tMPS is found to show the logarithmic scaling law, where the scaling coefficient gives the central charge that characterizes the criticality of the theory. Our work also implies that the spectra of the transfer matrices defined by the ground state and tMPS provide information of the low-lying masses of the theory in the continuous limit. This could help to understand the role of the finiteness of the bond dimension as an infra red regulator. Furthermore, we show from the perspective of methodology that, the tMPS emerges from a generalized TN ab-initio optimization principle scheme, which unifies the infinite density matrix renormalization group and the infinite time-evolving block decimation algorithms.

PACS numbers: 75.40.Mg, 71.27.+a, 11.25.Hf, 02.70.-c

I. INTRODUCTION

In the last three decades, strongly-correlated quantum many-body systems remain in the center of scientific interests and define the most important challenges and open questions[1–4]. For instance, understanding of certain classes of quantum many-body systems is necessary for the understanding of the mechanism of high-T_c superconductivity (cf.[5,6]), or of topological phase transitions (cf.[7,8]) and spin liquids (cf.[9], for the recent experiment see[10]). These systems are notoriously hard to be studied analytically or numerically. Exact solutions are extremely rare for such kind of systems. For this reason, novel efficient numerical approaches are highly desired.

One of the most important numerical tools developed in the last decades is the methods based on tensor network[11–14]. It offers an efficient representation of quantum many-body states that coincides with their entanglement structure. It takes advantage of the fact that not all quantum states in the Hilbert space of many-body systems (in particular with short-range interactions) are equally relevant for the low-energy and low-temperature physics. It has been found, namely, that the low-lying eigenstates of gapped Hamiltonians with local interactions obey the so-called area law of the entanglement entropy[15].

Most tensor network algorithms implement the philosophy of the renormalization group (RG). The best known algorithm in this sense is the density matrix renormalization group (DMRG)[16,17]. Based on the idea of Wilson's numeric RG[18], White proposed DMRG in 1992 to simulate the ground states of one-dimensional (1D) quantum systems. Its basic idea is to add one site to the block and its copy each time, then renormalize the Hilbert space by integrating out the basis of the less entangled part. Beyond its original target, DMRG has been extended with great success to simulate different finite-temperature thermal states[19–21] and two-dimensional (2D) quantum models of finite sizes[22], as well as to simulate quantum chemistry problems[23].

Besides RG terminology, DMRG is now better understood in the language of TN, i.e., matrix product states (MPS) and matrix product operators (MPO)[12,24,25]. Specifically, the ground state obtained by DMRG was found to be an MPS that indicates a renormalization flow of the Hilbert space. Such a new perspective stimulates us to implement DMRG in a more efficient way and provides new clues for further improvements, e.g., the central matrix technique to speed up the convergence[25,26], and a perturbation theory of DMRG to improve its accuracy[27]. Besides, MPS itself has also been proven to be extremely powerful as a variational ansatz for 1D quantum models defined on both discrete[12], and continuous space[28–31]. Beyond numerics, MPS has been shown to be an effective tool to analytically investigate, e.g., the exact representations of non-trivial states (see one of the early works in Ref.[32,33]), the entanglement scaling properties[34], etc.

The progress in understanding of entanglement entropy has prompted a series of new developments that extend the domain of the numeric RG methods. For this reason in 2004, Vidal proposed a new algorithm: the time evolving block decimation[35–37]. Using Trotter-Suzuki decomposition[38,39], the calculation of the ground state or the time evolution becomes the contraction of 2D tensor Network (TN), where the TN is contracted layer by layer to an MPS until the convergence is reached. After each contraction, the dimension of the MPS increases, and an optimal truncation is introduced to reduce the dimensions[40]. In this sense, TEBD solves the simulation in a contraction-and-truncation (C&T) way.

The C&T scheme is very popular and useful to compute not only ground states, but also general TN contraction prob-

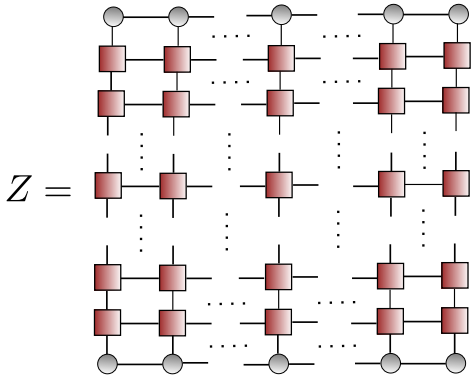

Figure 1. (Color online) Representation of 2D tensor network for the imaginary time evolution.

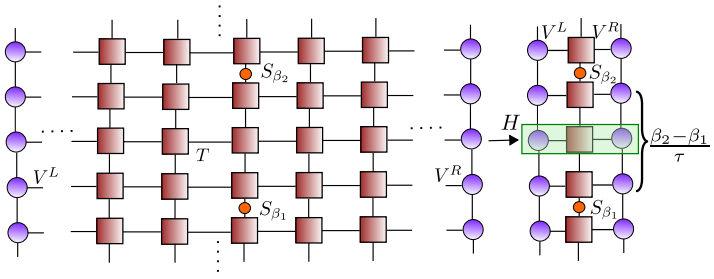

Figure 2. (Color online) The TN representation of the dynamic correlation function $\mathcal{C}(d\beta) = \langle \hat{S}_{\beta_1} \hat{S}_{\beta_2} \rangle$ with $d\beta = \beta_2 - \beta_1$ ($\beta_1 < \beta_2$), which can be calculated by the contraction of the tMPSs with an infinite TN stripe in the vertical direction.

lems. Compared to the DMRG idea, the C&T scheme is much easier to be generalized to simulate higher-dimensional systems. One famous example is tensor renormalization group (TRG)[41–52]. In TRG, the TN is deformed by singular value decomposition (SVD) and then contracted in a certain way so that the resulting TN restores its original geometry. After each contraction, the total number of tensors in the TN decreases and the bond dimensions of the tensors increase exponentially. Then truncations, which can be obtained locally (called simple or cluster update)[41–48] or non-locally (called full update)[49–52], are implemented to bound the dimensions. The main difference among these truncation schemes are the ways of keeping important basis by considering different environments, which lead to different accuracy and computational cost.

Another way to contract a TN is through the boundary methods. For the boundary methods an MPS is used as an ansatz for the environment. Early works of such boundary methods were proposed by Baxter: the corner transfer matrix (CTM)[53,54]. The CTM together with the DMRG algorithm served as an inspiration for Nishino et al to introduce CTMRG as a powerful boundary method for calculating 2D classical partition functions[55]. Then it was further developed by Orus et al to solve TN contractions[56,57].

Recently, an efficient boundary method, called *ab-initio* optimization principle (AOP), was suggested[58]. The AOP algorithm is inspired by both the bath-simulated method such as density matrix embedding theory and the CTM. The general idea of AOP is to encode an infinite TN into a local function with finite number of degrees of freedom. AOP leads to the few-body Hamiltonian[59] that consists of a finite bulk of the original system embedded in an entanglement bath that is determined by the fixed point of a set of self-consistent equations. In other words, the whole infinite TN contraction is "encoded" in the local eigenvalue equations. Two principles are followed: (i) the equations should be as simple as possible so that they can be efficiently simulated by classical computers; (ii) the equations should contain minimal number of input parameters, which are given by the local tensor.

In this work, we focus on the imaginary time evolution of one dimensional system and in particular in the criticality and excitations by an MPS emerging in the imaginary time direction called time MPS (tMPS). Some previous works have successfully used the tMPS or similar with a "folding" trick to build an efficient time-evolution algorithm[29,60]. The key difference here is that we enforce the translational invariance and show that the time MPS is a well-defined many-body state, like the ground state, which provides useful physical information of the system. With the TN for the ground-state simulations of 1D quantum systems, we show that the tMPS possesses the same structure of the continuous MPS originally proposed for the field theories[28]. Meanwhile, it respects the dual symmetry in our benchmark model, and exhibits the same properties as the spatial MPS (ground state). Moreover, the correlation of the tMPS gives the dynamic correlation of the ground state, from which the excitation gap can be accurately obtained. Furthermore, our work demonstrates that other than the ground state, tMPS can be an alternative way of revealing the properties of the many-body system. By studying the transfer matrices of the ground state and tMPS, we obtain the low-lying spectrum of the theory in the continuous limit, an important footprint that allows to understand the role of the bond dimension as an infrared regulator.

Finally, we explicitly build an equivalence between iDMRG[26] and iTEBD[37,40] in the AOP picture[58]. Note that these two important algorithms have been considered as two different schemes and their connections are barely discussed. Considering a 2D TN that can either represent a 2D classical partitioning or a (1+1)-dimensional quantum theory, we show that when we do iDMRG, which is the renormalization along the spatial direction, in fact we are doing iTEBD in the other direction simultaneously, and *vice versa*. Two MPSs are defined accordingly, which are the well-known MPS giving a real-space renormalization flow in iDMRG (dubbed as spatial MPS)[12], and a translationally invariant MPS in iTEBD in the vertical (imaginary time) direction.

This paper is organized as following. In Sec. II, we define the tMPS, giving the necessary formulation. In Sec. III, we demonstrate that the tMPS is continuous. In Sec. VI, we verify our scheme for different models, and show that the tMPS accurately reproduces the physical properties of the ground state. In Sec. VI, we explain the generalized AOP scheme that unifies iDMRG and iTEBD, and show how the tMPS emerges in such a scheme. In the appendix, we briefly review iDMRG

and iTEBD, and the standard AOP scheme.

II. BASIC DEFINITIONS AND PRELIMINARIES

In this work, we focus on the TN representation of (1+1)D of infinite size. In particular, we will evaluate the 2D TN shown in Fig. 1. Z can be the partition function of statistic models, or the time evolution (imaginary or real). More specifically, we will focus on calculating the imaginary time evolution of $|\psi\rangle$.

Let us take the 1D system of N sites with the Hamiltonian $\hat{H} = \sum_n \hat{H}^{[n,n+1]}$ as an example, where $\hat{H}^{[n,n+1]}$ gives the two-body interactions. Here, we impose translational invariance, i.e., $\hat{H}^{[n,n+1]} = \hat{H}^{[2]}$. The variational ground state can be reached through various schemes, for example, to implement imaginary time evolution in a randomly initialized matrix product state (MPS) (see the Appendix A 1 for more details) to minimize the ground state energy

$$\min\langle\psi|\hat{H}|\psi\rangle = \lim_{\beta\to 0}\langle\psi|e^{-\beta\hat{H}}|\psi\rangle. \tag{1}$$

Practically, this procedure has to be equipped with Trotter-Suzuki decomposition because of the non-commuting two-body terms in the Hamiltonian $\hat{H}$.

Then starting from the local Hamiltonian $\hat{H}^{[2]}$, the tensor that forms that TN as shown in Fig. 1 can be defined in different ways. For example, one way is to decompose the local evolution operator as $U_{\sigma_1\sigma_2\sigma_1'\sigma_2'} = \langle\sigma_1'\sigma_2'|e^{-\tau\hat{H}^{[2]}}|\sigma_1\sigma_2\rangle = \sum_\alpha U^L_{\sigma_1\sigma_1'\alpha}U^R_{\sigma_2\sigma_2'\alpha}$, with τ the Trotter step. Then the tensor in the TN is defined as

$$T_{\sigma\alpha\sigma'\alpha'} = \sum_{\sigma_1''\sigma_2''} U_{\sigma_1'\sigma_2'\sigma_1''\sigma_2''}U^L_{\sigma_1\sigma_1''\alpha}U^R_{\sigma_2\sigma_2''\alpha'}, \tag{2}$$

with $\sigma = (\sigma_1, \sigma_2)$ and $\sigma' = (\sigma_1', \sigma_2')$.

Normally, the ground-state simulation is implemented by contracting the TN along the imaginary time direction. Then the boundary MPS stretching along the real-space direction is obtained as the ground state. Similarly, the tMPS can be defined as the boundary MPS along the imaginary time direction as (Fig. 2)

$$|tMPS\rangle = \sum V^{L(R)}_{\alpha_i\beta_i\beta_{i+1}}\cdots V^{L(R)}_{\alpha_j\beta_j\beta_{j+1}}|\alpha_i\cdots\alpha_j\cdots\rangle \tag{3}$$

The tMPS can be calculated by directly contracting along the real-space direction, as Ref.[29,60] did. In Sec. V, we show how the tMPS emerges in a generalized AOP scheme, where the tensor $V^{L(R)}$ is solved in a set of self-consistent eigenvalue problems.

III. THE CONTINUOUSNESS OF THE TIME MPS

When the TN represents a system where the horizontal and vertical directions are equivalent to each other, the two MPSs in the two directions are identical to each other. The possible difference is given by gauge transformations, i.e., the parallel MPS is in the central canonical form (because of the iDMRG algorithm) and the vertical one is in the canonical form when choosing the proper gauge. The discussions about different canonical forms can be found in the Appendix. This equivalence has been tested on the TN that gives the partition function of the 2D classical Ising model (see the Appendix B).

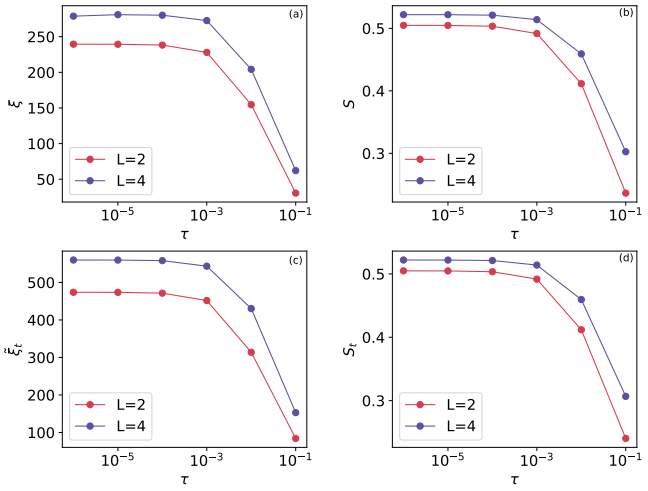

Figure 3. For the spatial MPS that gives the ground state of the Hamiltonian, the correlation length ξ and the entanglement entropy S of the spatial MPSs converge when the Trotter step τ decreases. We obtain analogous results for the tMPS. We take the length of the unit cell $L = 2, 4$ and the bond dimension cut-off $\chi = 20$.

Interestingly, when the TN represents the imaginary-time evolution of a 1D quantum chain or even higher-dimensional quantum systems, the two directions might no longer be equivalent. One difference is that the parallel direction is characterized by the lattice spacing unit that is discrete, and the vertical direction is the imaginary time that is actually continuous. In this case, the parallel MPS is the ground state, as expected, and the *time MPS* should be a continuous MPS (cMPS)[28].

We take quantum Ising chain as an example, where the Hamiltonian reads

$$H = J\sum_i S_i^x S_{i+1}^x - h\sum_i S_i^z, \tag{4}$$

with S^x and S^z the spin operators on the x and z directions. The model has been exactly solved by fermionization[61]. The system is in a paramagnetic phase for $h/J > 1.0$ with an order parameter $\langle S^z\rangle \neq 0$, and in a ferromagnetic phase for $h/J < 1.0$ with order parameters go to zero. In the infinite case a quantum phase transition occurs at $h/J = 1.0$ where the system has central charge $c = 0.5$.

The first evidence we observed is the correlation length. The (well-known) general way of calculating the correlation length of a translationally invariant MPS is illustrated in Fig. 2. Eventually, it is determined by the gap of the transfer matrix of the MPS as

$$\xi = \frac{1}{\ln\eta_0 - \ln\eta_1}, \tag{5}$$

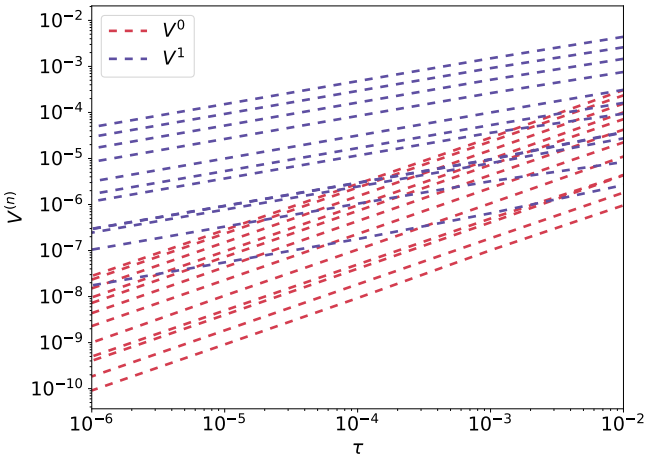

Figure 4. We show the components of the tMPS, V^0 and V^1 [Eq. (7)]. Each line represents a different components of the two tensors for 1D transverse Ising chain at the critical magnetic field. Our results suggest that the tMPS can be accurately obtained from the cMPS.

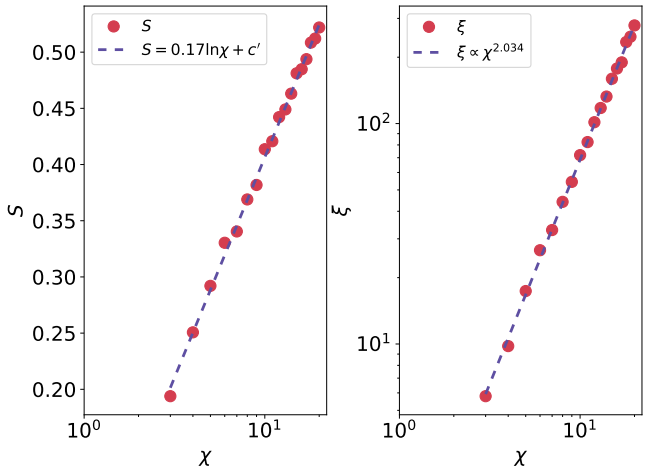

Figure 5. (Color online) The scaling of the correlation length ξ and entanglement entropy S versus the bond dimension cut-off χ of the spatial MPS. We take $h = 0.5$, $L = 2$ and $\tau = 10^{-6}$.

with η_n the n-th eigenvalue of the transfer matrix. More details can be found in Appendix A 5.

In Fig. 3, we show the correlation length ξ and entanglement entropy S of the spatial MPS, which converges rapidly to finite values as the Trotter step τ decreases [Fig. 3 (a) and (b)]. The correlation length ξ_T of the obtained directly from the tMPS [Eq. (5)] diverges as τ decreases, thus is not well-defined. Considering that the (imaginary) time length is determined by both ξ_T and the Trotter step τ that characterizes the discretization of time, the (physical) time correlation length should be defined as $\tilde{\xi}_T = \xi_T \tau$. Fig. 3 (c-d) show that $\tilde{\xi}_T$ and S converge rapidly when reducing τ.

To further verify the continuousness of the tMPS, we compare its structure with the cMPS. The cMPS was firstly proposed by Verstraete *et al*[28]. Before this, the continuous limit of MPS was discussed and utilized with Bethe ansatz[62,63]. This family of states represents the continuous limit of standard MPS. The cMPS can be used as the variational states for finding ground states of quantum field theories, as well as to describe real-time dynamical features. Just as MPS captures the entanglement structure of low-energy states of quantum spin systems, the cMPS seems to capture the entanglement features of the low-energy states of quantum field theories. The cMPS has the structure as

$$|\psi\rangle = \sum_{\sigma_1 \cdots \sigma_L} V^{\sigma_1} \cdots V^{\sigma_L} \left(\Psi_1^\dagger\right)^{\sigma_1} \cdots \left(\Psi_L^\dagger\right)^{\sigma_L} |\Omega\rangle, \quad (6)$$

with the specific structure of the tensor satisfying

$$V^0 = I - \tau Q \quad (7)$$

$$V^1 = \tau R \quad (8)$$

$$V^n = \tau^n R^n \quad (9)$$

$$\Psi = \frac{\hat{a}_i}{\sqrt{\tau}}. \quad (10)$$

with τ a small constant that approaches to zero.

In particular, we study the structure of tMPS obtained from the quantum Ising chain. In Fig. 4 we show the components V^0 and V^1 in function of τ, verifying Eqs. (7) and (8). For higher orders of τ, it is too small to verify when $\tau < 10^{-3}$. This implies that by performing an appropriate scaling analysis, we can extract directly the continuous MPS by performing a simple extrapolation with the appropriate τ dependence to the interesting $\tau \to 0$ limit, without using the continuous ansatz directly that is notoriously difficult to optimize.

IV. CRITICALITY

It is known[64–68] that while using MPS to approximate the ground state at the critical point, the correlation length satisfies an algebraic scaling against χ as

$$\xi \propto \chi^{\kappa}. \quad (11)$$

And its entanglement entropy S fulfills logarithmic scaling laws versus the correlation length ξ and dimension cut-off χ as

$$S = \frac{c\kappa}{6} \ln \chi + c', \quad (12)$$

$$S = \frac{c}{6} \ln \xi + c'. \quad (13)$$

For the spatial MPS, our results with $L = 2$ (L is the size of the unit cell in the AOP calculations, see the Appendix) precisely demonstrate such behaviors given by Eqs. (11) and (12) (Fig. 5). In Fig. 6, the scaling of S against ξ of the spatial MPS with $L = 2$ and 4 is given. The results accurately give the central charge $c = 0.5$ with an error $O(10^{-3})$. Note that for different choices of L, there are small corrections to both ξ and S versus χ, leading together to better results of c.

Close to the critical point, the systems becomes not only scale invariant but also Lorentz invariant (this is equivalent to

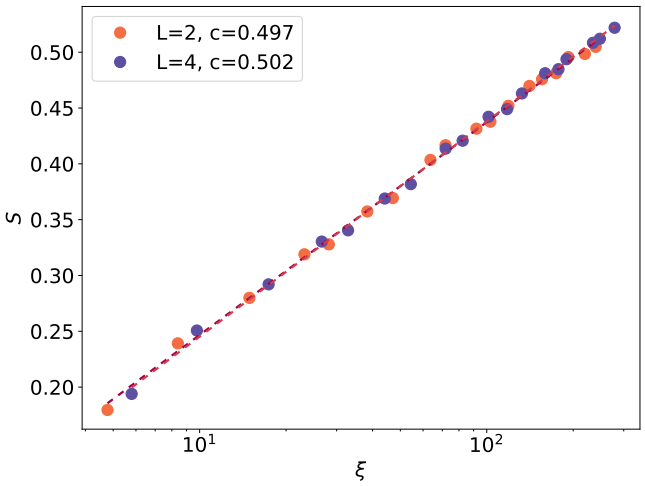

Figure 6. (Color online) By varying the dimension cut-off χ and the size of the unit cell L, the entanglement entropy S against correlation length ξ of the ground state of 1D transverse Ising chain at the critical magnetic field is given. An intrinsic logarithmic scaling behavior is observed, which is independent of calculation parameters. The central charge c from the fitting with different L is accurately obtained (with the exact solution $c = 0.5$).

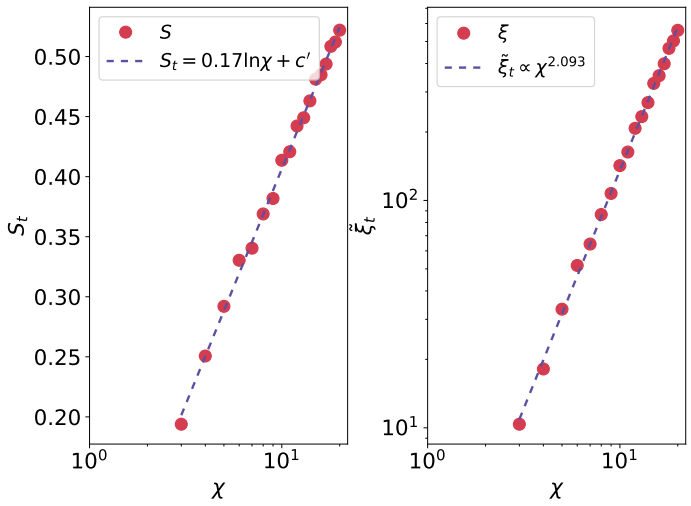

Figure 7. (Color online) The scaling of the dynamic correlation length $\tilde{\xi}_T$ and the temporal entanglement entropy S_T versus the bond dimension cut-off χ of the tMPS. We take $h = 0.5$, $L = 2$ and $\tau = 10^{-6}$. Both exhibit a critical behavior at the critical point.

the Galileo invariance in Euclidean time), as a consequence of the linear dispersion relation for low-energy excitations. For this reason it is possible to rotate the system and invert the role of space and time. In this way we can think of the tMPS as a state along the infinite time direction, and we expect it to share some properties (e.g. the scaling exponents) with the matrix-product state defined along the spatial direction.

As shown in Fig. 7, we can extract the correlation length $\tilde{\xi}_T$ and the entanglement entropy S_T of the tMPS (also dubbed as temporal entanglement[29]), where we find that $\tilde{\xi}_T$ and S_T also satisfy Eqs. (11) and (12), respectively, same to the ground state. From our best fit, we extract $\kappa = 2.026$ and $c_T = 0.5$ for the tMPS. The scaling between ξ and S_T also satisfies Eq. (13) and gives the same value for the central charge (Fig. 8), as expected. Interestingly, despite the fact that the tMPS is continuous, the entropy is finite, a consequence of the fact that the bond dimension plays the role of an UV regulator, as already observed in[28]. As expected, thus the continuum limit results in a massive state, where the masses should be dictated by the Ising fixed point.

From the classical perspective, the present phenomenon is equivalent to the well known fact in $2D$ anisotropic Ising model, where the coupling along the space direction J_s is different from the coupling along the time direction J_t. The model indeed possesses a line of critical points, defined by the equation $\sinh(2\beta J_t)\sinh(2\beta J_s) = 1$, where β is the inverse temperature (see, e.g.[69]). As a consequence, and as expected we indeed see that

$$\xi = \nu\tilde{\xi}_T, \tag{14}$$

with ν a constant. Such a relation is also verified, e.g., at the critical point, as shown in Fig. 8. Interestingly, we find that $\tilde{\xi}_T$ is twice as ξ, something that from the analogy with the classical Ising model is unexpected, since the critical line is indeed obtained by equating the space and time correlation lengths. A first possibility is that factor 2 could just encode the a non-universal effect on the speed of excitations. If this was the case, we would expect that all the gaps of the time transfer matrix should be double the gaps of the space transfer matrix. We thus proceed to compare the higher spectrum of the two matrices. We define

$$\tilde{\xi}_T^{(n)} = \frac{1}{\tilde{\Delta}_n} = \left(\log\frac{\tilde{\eta}_0}{\tilde{\eta}_n}\right)^{-1}, \tag{15}$$

$$\xi^{(n)} = \frac{1}{\Delta_n} = \left(\log\frac{\eta_0}{\eta_n}\right)^{-1}, \tag{16}$$

where η and $\tilde{\eta}$ are the eigenvalues of the spatial and time transfer matrix. Note for $n = 1$, we have that $\tilde{\xi}_T^{(1)} = \tilde{\xi}_T$ and $\xi^{(1)} = \xi$. With different χ (Fig. 8) we found that all gaps of the time transfer matrix are indeed proportional to the gaps of the spatial transfer matrix. However the proportionality constant does not depend on the particular gap and it is always the same. This result can be interpreted as a non-universal renormalization of the velocity.

In order to understand these results we can get inspired by the results of the spectrum of a conformal field theory (CFT) in a finite size geometry originally obtained by Cardy in a series of famous papers[70,71]. In those papers, it is explained how the boundary conditions of the system play an important role in defining which sectors are present in the spectrum of the transfer matrix of a critical Ising model. These result have been confirmed in numerical simulations several times, by using finite-size scaling analysis on small systems[72] and more recently the MERA[73]. In particular we would like to understand if the discrepancy between the two spectra can be attributed to the fact that the system has different boundary conditions along the space and the time direction.

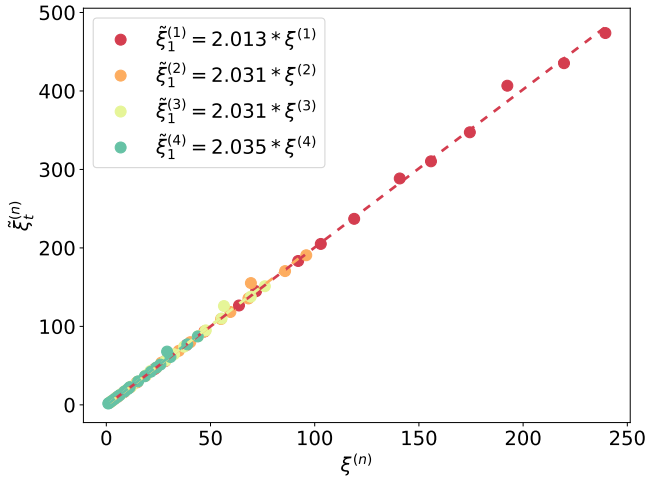

Figure 8. (Color online) Correlation length of the tMPS $\tilde{\xi}_T^{(n)}$ versus that of the spatial MPS $\xi^{(n)}$ for different bond dimension χ at $\tau = 10^{-6}$. Both spectra depends linearly on W_A defined in the main text. Our results suggest that $\tilde{\xi}_T^{(n)} = \alpha\xi^{(n)}$ with $\alpha = 2$.

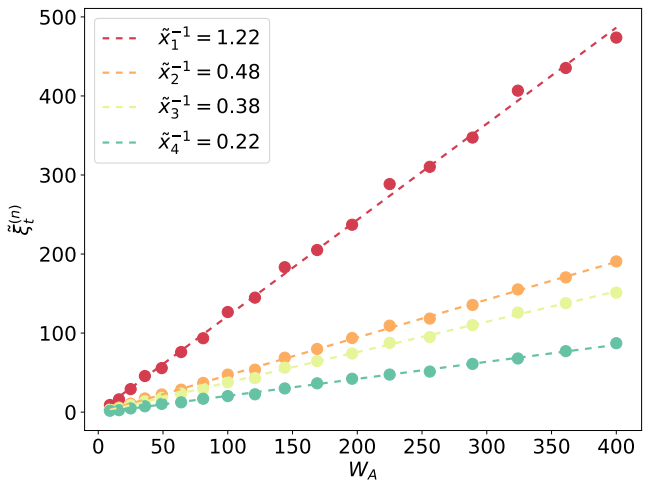

Figure 9. (Color online) Correlation length of the tMPS $\tilde{\xi}_T^{(n)}$ versus $W_A \simeq \chi^2$ at $\tau = 10^{-6}$. A linear relation is discovered and the slopes can be used to unveil the spectrum of the low-energy theory. The results are different from those known for the Ising universality class and seem to suggest that the finite bond dimension can be used as a regulator to obtain a non-trivial continuum limit close to the Ising critical point.

The analysis of the spectrum of the space transfer matrix was already performed in[68] and we thus refer the reader to that paper for the related discussion. Here we focus on the analysis of the time transfer matrix. Using as a guidance the CFT results we assume the following scaling form the spectrum of the time transfer matrix

$$\Delta_n = \tilde{x}_n / W_A. \tag{17}$$

where W_A is related to a relevant operator opening the gap. $\tilde{x}_n$ are the exponents of the scaling fields selected by the boundary conditions[70,71]. For a system defined on a cylinder of circumference L for example $W_A = L/(2\pi)$.

In Fig. 9 we show that a legitimate choice of W_A is $W_A \simeq \chi^2$, since as a function of that variable the corresponding inverse gaps grow linearly. However the lack of analytical results about the explicit expression of W_A renders the identification of the spectrum $\tilde{x}_n$ of the theory and its connections with the expected CFT spectra difficult (see a related discussion in[68]). Rather than on the actual value of the gaps we thus focus on their ratios that should be independent on the proper definition of W_A but should encode the ratios of $\tilde{x}_n/\tilde{x}_1$. For example depending on the boundary conditions these ratios in the Ising CFT are $8, 9, 9$ for PBC, $3, 4, 5$ in the case of the Free Boundary conditions, and $1.5, 2, 2$ for the case of Fixed boundary conditions. With our numerical results we can extract the pre-factors of the gaps in an increasing order as $\alpha\tilde{x}_1 = 1/1.21 \simeq 0.83$, $\alpha\tilde{x}_2 = 1/0.48 \simeq 2.083$, $\alpha\tilde{x}_3 = 1/0.38 \simeq 2.63$ and $\alpha\tilde{x}_4 = 1/0.22 \simeq 4.55$ with α an unknown constant. We get rid of α by taking the rations $\tilde{x}_2/\tilde{x}_1 = 2.51$, $\tilde{x}_3/\tilde{x}_1 = 3.17$, $\tilde{x}_4/\tilde{x}_1 = 5.48$, that do not match any of the expected spectra. Due to the fact that the finite bond dimension explicitly breaks the Z_2 symmetry, we could expect that the above masses are due to the presence of a magnetic perturbation rather than a thermal one as in the case of a finite geometry. The only result in this direction we are aware of is the famous E_8 spectrum obtained by using Zamolodchikovs conjecture[74,75] that reads $\tilde{x}_2/\tilde{x}_1 = 1.6$, $\tilde{x}_3/\tilde{x}_1 = 1.9$, $\tilde{x}_4/\tilde{x}_1 = 2.4$. Unfortunately also these ratios are significantly different from the ones we obtain. For related results away from the critical temperature check also[76,77].

We thus leave to further studies the identification of the spectra of the theory in the continuum limit, that will be very relevant in order to understand the real role of the infrared regulator in the tMPS. Our results thus seem to suggest the existence of a new non-trivial continuum limit close to the Ising critical point. In Fig. 10, we show the indeed that the entanglement entropy vs the effective correlation length $\tilde{\xi}_T$ of the tMPS are related through the correct central charge $c_T = 1/2$; this is the confirming the equivalence between space and time.

Moreover, it is known in presence of the gap the dynamical correlation function decay exponentially with the excitation gap Δ. Thus, the excitation gap can be given by the dynamic correlation length as

$$\Delta \propto |h - h_c| \propto \frac{1}{\tilde{\xi}_T}. \tag{18}$$

In Fig. 11, we show the excitation gap obtained from the tMPS by using Eq. (18). By fitting, the critical point where the gap vanishes is accurately determined. Our simulations robustly show that the tMPS is a well-defined continuous many-body state that can be used to obtain physical information of the system.

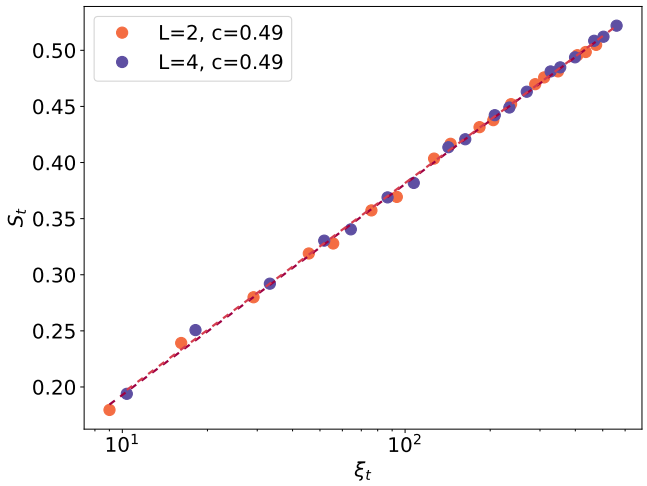

Figure 10. (Color online) By varying the dimension cut-off χ and the size of the unit cell L at $\tau = 10^{-6}$, the temporal entanglement entropy S_T against effective correlation length $\tilde{\xi}_T$ of the tMPS of 1D transverse Ising chain at the critical magnetic field is given. An intrinsic logarithmic scaling behavior is observed, which is independent of calculation parameters. The central charge c_T obtained from the tMPS is the same as the ground state, which is consistent with the equivalence between space and time in this model.

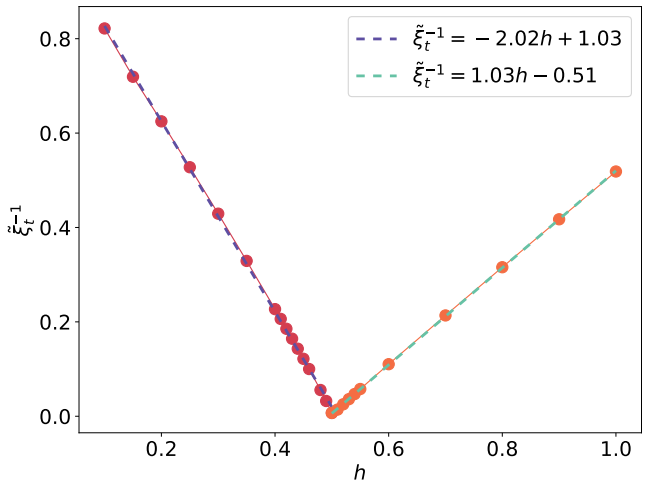

Figure 11. (Color online) The inverse of the correlation length $\tilde{\xi}_T$ of the tMPS is found to bear a linear relation with h at $\tau = 10^{-6}$. According to Eq. (18), our results suggest that the excitation gap can be accurately obtained from the correlation length of the tMPS.

V. METHOD: A GENERALIZED TENSOR NETWORK ENCODING

In this section, we revisit iDMRG (specifically the one developed in[26]) and iTEBD, and show that these two different algorithms can be unified in a generalized TN encoding scheme, where the tMPS naturally emerges. Here, we take the one-site iDMRG as example. Comparing with the standard TN encoding algorithm where all eigenvalue problems are required to be Hermitian (see the Appendix A 4 in detail), the TN encoding given by iDMRG allows for non-Hermitian matrices. Still, the general idea remains the same, where the infinite TN contraction is encoded into local eigenvalue problems.

As shown in Fig. 12 (a), (b) and (c), there are three local eigenvalue equations, which are given by three matrices

$$M^L_{s_2b_1b_1',s_4b_2b_2'} = \sum_{s_1s_3} T_{s_1s_2s_3s_4} A^*_{s_1b_1b_2} A_{s_3b_1'b_2'}, \quad (19)$$

$$M^R_{s_2b_1b_1',s_4b_2b_2'} = \sum_{s_1s_3} T_{s_1s_2s_3s_4} B^*_{s_1b_1b_2} B_{s_3b_1'b_2'}, \quad (20)$$

$$\mathcal{H}_{s_1a_1a_2,s_3a_1'a_2'} = \sum_{s_2s_4} T_{s_1s_2s_3s_4} V^L_{s_2a_1a_1'} V^R_{s_4a_2a_2'}. \quad (21)$$

V^L, V^R and Ψ are the eigenstate of these three matrices that respectively satisfy

$$\sum_{sb_1b_1'} V^L_{sb_1b_1'} M^L_{sb_1b_1',s'b_2b_2'} \propto V^L_{s'b_2b_2'} \quad (22)$$

$$\sum_{s'b_2b_2'} M^R_{sb_1b_1',s'b_2b_2'} V^R_{s'b_2b_2'} \propto V^R_{sb_1b_1'} \quad (23)$$

$$\sum_{s'a_1'a_2'} \mathcal{H}_{sa_1a_2,s'a_1'a_2'} \Psi_{s'a_1'a_2'} \propto \Psi_{sa_1a_2}. \quad (24)$$

Eqs. (19) and (20) need not be Hermitian.

A and B, which are the left and right orthogonal part of Ψ, are obtained by QR decomposition [Fig. 12 (d)] as

$$\Psi_{sa_1a_2} = \sum_{a'} A_{sa_1a'} \tilde{\Psi}_{a'a_2} = \sum_{a'} \tilde{\Psi}^\dagger_{a_1a'} B_{sa'a_2}, \quad (25)$$

where A and B are isometries, satisfying orthogonal conditions as

$$\sum_{sa} A_{saa_1} A^\dagger_{saa_2} = I_{a_1a_2}, \quad (26)$$

$$\sum_{sa} B_{sa_1a} B^\dagger_{sa_2a}. = I_{a_1a_2}. \quad (27)$$

The above scheme can be reinterpreted in the iDMRG language. V^L and V^R represent the system and environment super-block. $\mathcal{H}$ is the effective Hamiltonian (note that instead of using the MPO of Hamiltonian, here in AOP, we use the operator $e^{\tau \hat{H}}$) with Ψ its ground state. By the QR decompositions on Ψ, the renormalization of the basis of the system and environment are given by A and B, and $\tilde{\Psi}$ is the center matrix[25,26].

Similarly to the AOP, the original TN can be reconstructed by repeatedly using the eigenvalue equations. We start from a local contraction (a scalar Z) of T and the boundary tensors as shown at the bottom of Fig. 13. Then with Eqs. (22) and

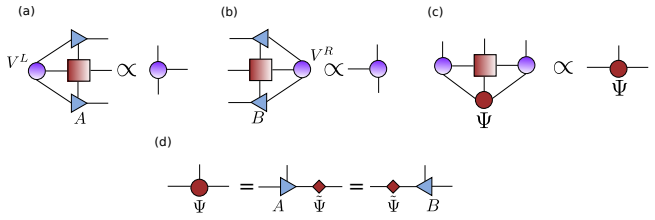

Figure 12. (Color online) The (a), (b) and (c) show the three local eigenvalue equations given by Eqs. (19, 20, 21). The isometries A and B are obtained by the QR decompositions of Ψ in two different ways, as shown in (d).

(23), Z is transformed to the product of an MPO with an MPS and its conjugate. One can see that like iDMRG, the MPS is formed by A's on the left side (left-orthogonal part) and B's on the right side (right-orthogonal part) with the center matrix $\tilde{\Psi}$ in the middle. Then by using the fact that such an MPS optimally gives the ground state, we can use the corresponding eigenvalue equation to reconstruct the entire TN (Fig. 13).

In the encoding, there are three constraints: the normalizations of V^L, V^R and the MPS. The first two constraints are obviously local with $\langle V_L|V_L\rangle = 1$ ($\langle V_R|V_R\rangle = 1$). For the third one, by utilizing the orthogonal conditions of A and B, the normalization of the MPS is equivalent to that of Ψ, which is also local. Then the equations like those in Fig. 12 (c) and (d) are no longer needed in this case. Thus, all eigenvalue problems are local and regular.

In the above scheme, one can explicitly see that V^L (or V^R) also gives an MPS, and interestingly, such an MPS is updated in the way of iTEBD contracting along the spatial direction. Let us pay attention to the eigenvalue equation that V^L satisfies Eq. (22). If one chooses to solve it using a power method, i.e. to find the ground state of M^L by updating V^L with the product $V^L M^L$, such a product is equivalent to evolving the local tensor of the MPS in iTEBD with the MPO formed by T in the vertical direction. In the evolution, the bond dimension of the local tensor V^L increases exponentially. Then, truncation is implemented by contracting with the isometry A. The TN encoding shows that while implementing iDMRG to get the MPS along the real-space direction, one is actually implementing iTEBD that gives the tMPS along the imaginary-time (or vertical) direction. We notice that some interesting discussions about the relations between (real-space) DMRG and the optimization of the real-space MPS were given[90]. These relations can be further applied to the tMPS using our proposal.

Note that A is obtained from the QR decomposition of Ψ. Considering the eigenvalue equation Eq. (24), Ψ in fact represents one half of the infinite environment of the vertical MPS, thus A gives the optimal truncation matrix. Considering that the evolution of V^L in the language of iTEBD is non-unitary, one important difference between the AOP and the iTEBD contracting in the spatial direction[60] is that the explicit implementation of canonicalization[40] is no longer necessary thanks to the eigenvalue equation Eq. (24). All these arguments also apply to V^R and B.

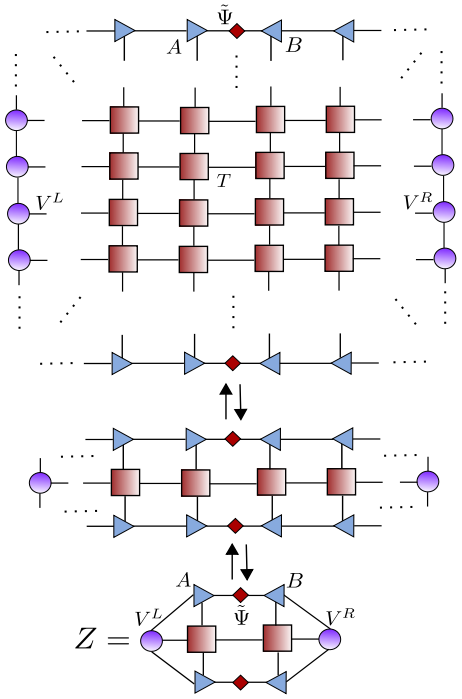

Figure 13. (Color online) The TN encoding given by iDMRG, where the TN contraction is equivalently transformed into a 1D TN and then finally into a local contraction.

The algorithm is implemented in the following steps:

- **Step 1:** From the Hamiltonian $\hat{H}$, define the local tensor T; give an initial guess of the tensor Ψ.

- **Step 2:** Calculate M^L and M^R; solve their dominant left and right eigenstates V^L and V^R, respectively. One may use the tensors obtained from the last iteration as the initial guess. Since M^L and M^R are not Hermitian, we update V^L and V^R as $V^L \leftarrow V^L(M^L)^n$ and $V^R \leftarrow (M^R)^n V^R$. The algorithm exactly becomes iDMRG (as we argued above) when taking the integer $n = 1$. It is also allowed to take $n > 1$, which speeds up the convergence. But possible instability may appear as n increases due to the non hermitian effective Hamiltonian.

- **Step 3:** Calculate the effective Hamiltonian $\mathcal{H}$ and its eigenstate Ψ. Again, one can use the A obtained in the last iteration as the initial guess. Obtain A and B by the QR decompositions of Ψ.

- **Step 4:** Check if A converges. If it does, proceed to Step 5. If not, go back to Step 2.

- **Step 5:** Use the tensors Ψ, A and B to construct the spatial MPS, and $V^{L[R]}$ for the tMPS; calculate the interested physical quantities, such as energy and entanglement.

VI. CONCLUSION

In this work, we propose to extract physical information of the 1D quantum systems from the an MPS defined in the imaginary time. In the generalized AOP scheme, the time MPS (tMPS) naturally emerges in the imaginary time direction of the TN, as a boundary MPS. We show that tMPS is continuous, which exhibits the same structure as the continuous MPS proposed for field theories. The information of excitations, e.g., dynamic correlation length and gap, can be accurately calculated from the tMPS. At the critical point, the tMPS is found to show the logarithmic scaling law, determined by the central charge that characterizes the criticality of the theory. By studying the transfer matrices of the ground state and tMPS, we obtain different ratios from their eigenvalues, which implies non-trivial dependence on the boundary conditions.

ACKNOWLEDGEMENTS

We thank Ian McCulloch for stimulating discussions. L.T. acknowledges the discussion with Giuseppe Mussardo and Pasquale Calabrese on the mass spectrum of the perturbed Ising model. S.J.R. acknowledges Fundació Catalunya - La Pedrera · Ignacio Cirac Program Chair. We acknowledge the Spanish Ministry MINECO (National Plan 15 Grant: FISICATEAMO No. FIS2016-79508-P, SEVERO OCHOA No. SEV-2015-0522, FPI), European Social Fund, Fundaci Cellex, Generalitat de Catalunya (AGAUR Grant No. 2017 SGR 1341 and CERCA/Program), ERC AdG OSYRIS, EU FETPRO QUIC, and the National Science Centre, Poland-Symfonia Grant No. 2016/20/W/ST4/00314.

Appendix A: Algorithms

In this section, we briefly review the formulation of iDMRG[16,17,78] and iTEBD[35,36]. In particular, we explain how to use these two algorithms to simulate the ground state of a 1D quantum system in the thermodynamic limit. The real-space renormalization of the physical Hilbert space is the key aspect in iDMRG. The ground state MPS is not explicitly translationally invariant, and actually represents a renormalization flow. Different from iDMRG, the iTEBD follows the C&T scheme, where the ground state wave function has an infinite MPS form made of a small number of tensors that are repeated indefinitely. To obtain the optimal truncation, one transforms the MPS in its canonical form and truncates the basis according to the canonical Schmidt numbers. In this way, the truncation error is minimized.

Moreover, we briefly review the standard AOP where the matrices appearing in the eigenvalue equations are assumed to be Hermitian. Then, by employing the idea of DMRG, we modify the eigenvalue equations to get rid of the Hermitian assumption, generalizing AOP for non-Hermitian problems. In this modified scheme, we show that two iMPSs appear along the two directions in the encoding of the 2D TN: one is the iMPS of iDMRG that represents an RG flow, and the other is the translationally invariant iMPS of iTEBD. In other words, the RG transformations in iDMRG are actually the truncations of the iMPS in iTEBD. It means that when iDMRG is implemented in one direction, in fact iTEBD is implemented at the same time in the other direction.

1. Infinite Matrix Product State

Here, we consider a 1D quantum chain. The physical degrees of freedom on each site give a local d-dimension Hilbert space $\mathcal{H}_d = \mathcal{C}^d$, where the local basis are denoted as $|\sigma_j\rangle$. A general form of a pure state can be written as

$$|\psi\rangle = \sum_{\sigma_1 \ldots \sigma_L} C_{\sigma_1 \ldots \sigma_L} |\sigma_1 \ldots \sigma_L\rangle, \tag{A1}$$

with $C_{\sigma_1 \ldots \sigma_N}$ coefficients of the state. One can see that the size of this high-rank tensor increases exponentially with the number of sites. To resolve such an "exponential wall", it has been proposed to write $C_{\sigma_1 \ldots \sigma_N}$ in an MPS form[11,12,24] that reads

$$|\psi\rangle = \sum_{\{\sigma\}} \sum_{\{\beta\}} A^{\sigma_1}_{1,\beta_1} A^{\sigma_2}_{\beta_1,\beta_2} \ldots A^{\sigma_L}_{\beta_{L-1},1} |\sigma_1 \ldots \sigma_L\rangle, \tag{A2}$$

where $A^{\sigma_i}_{\beta_{i-1},\beta_i}$ is a third-order tensor, i.e., a $(\chi_{i-1} \times \chi_i)$ matrix for each value of σ_i (χ_i the bond dimension of the virtual index β_i). Such a representation can be readily generalized to infinite systems with translationally invariant MPS, i.e. $A^{\sigma_l}_{\beta\beta'} = A^{\sigma}_{\beta\beta'}$ for $\forall \sigma_l$. (see Fig. 14).

Given a quantum state, its MPS representation is in general not unique, but it has gauge degrees of freedom. For each virtual bond β_i, we can define an invertible square matrix X_i, and rewrite the state Eq. (A2) by inserting an identity in each virtual bond as

$$\begin{aligned} &\ldots A^{\sigma_1}_{1,\beta_1} A^{\sigma_2}_{\beta_1,\beta_2} \ldots A^{\sigma_l}_{\beta_{l-1},\beta_l} \ldots = \\ &\ldots X_1 \left(X_1^{-1} A^{\sigma_2}_{\beta_1,\beta_2} X_2 \right) \ldots \left(X_{l-1}^{-1} A^{\sigma_l}_{\beta_{l-1},\beta_l} X_l \right) \ldots . \end{aligned} \tag{A3}$$

The new MPS is formed by B that is again a $d \times \chi_{l-1} \times \chi_l$ tensor satisfying

$$B^{\sigma_l} = X_{l-1}^{-1} A^{\sigma_l} X_l. \tag{A4}$$

The MPS Eq. (A2) is then written as

$$|\psi\rangle = \sum_{\{\sigma\}} \ldots B^{\sigma_1} B^{\sigma_2} \ldots B^{\sigma_l} \ldots |\sigma_1 \ldots \sigma_l \ldots\rangle, \tag{A5}$$

which gives exactly the same state as that formed by A. Therefore, the gauge of MPS is equivalent to the direct sum of the groups of isomorphisms of χ_l dimensioned complex vector spaces

$$\mathcal{G}_{MPS} = \oplus_{l=1}^{\infty} \mathrm{Iso}\left(\mathcal{C}^{\chi}\right). \tag{A6}$$

To fix the gauge, one can define the left-normalized form of the MPS, where the local tensor satisfies

$$\sum_{\sigma} A^{\sigma\dagger} A^{\sigma} = I. \tag{A7}$$

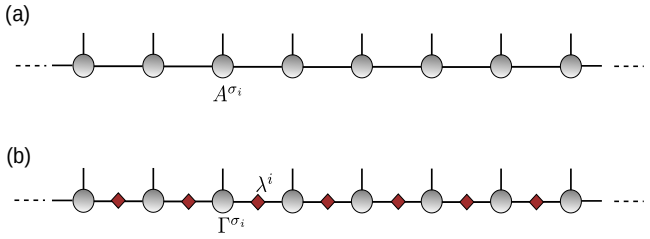

Figure 14. Graphical representation of an infinite matrix product state (MPS). In (a) the tensors A^{σ_i} are in left canonical form (right canonical form). In (b) we show the infinite matrix product state (MPS) in Vidal's formulation. Γ is the local tensor while λ represents the entanglement of the system.

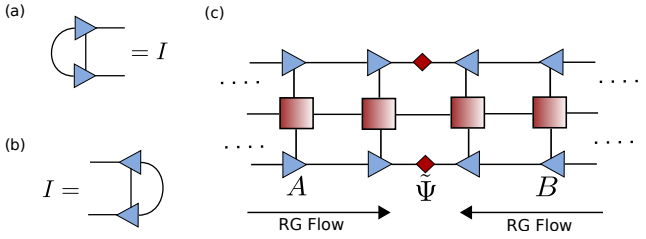

Figure 15. (Color online) The orthogonal conditions of the isometries (a) A and (b) B. (c) The MPS that appears in DMRG is formed by A, B and $\tilde{\Psi}$. Such an MPS is in the orthogonal form and gives a RG flow in the physical space of the Hamiltonian H.

Similarly, the right-normalized form is defined as

$$\sum_{\sigma} B^{\sigma} B^{\sigma\dagger} = I. \tag{A8}$$

To have the translational invariance, an MPS with a positive-defined diagonal matrix on each virtual bond is introduced as (see Fig. 14 (b))

$$|\psi\rangle = \sum_{\sigma_1 \ldots \sigma_L} \Gamma^{\sigma_1}\Lambda^{[1]}\Gamma^{\sigma_2}\Lambda^{[2]}\cdots\Gamma^{\sigma_{l-1}}\Lambda^{[l-1]} \Gamma^{\sigma_l}\Lambda^{[l]}\cdots\Gamma^{\sigma_{L-1}}\Lambda^{[L-1]}\Gamma^{\sigma_L}|\sigma_1\cdots\sigma_L\rangle. \tag{A9}$$

In this way, the canonical form of an MPS can be defined, which is connected with the left and right orthogonal form by

$$A^{\sigma_l} = \Lambda^{[l-1]}\Gamma^{\sigma_l}, \quad B^{\sigma_l} = \Gamma^{\sigma_l}\Lambda^{[l]}. \tag{A10}$$

In this form, one can prove that Λ is actually the bipartite entanglement spectrum of the state.

2. Infinite density matrix renormalization group

In the DMRG scheme, one typically starts with a short block (of length l) dubbed as the system (S) and its copy as the environment (E). The basis are denoted as $\{|\alpha_l^S\rangle\}$ and $\{|\alpha_l^E\rangle\}$, respectively. Then one grows the chain to add two sites between the system and the environment. Then the total state can be written as

$$|\psi\rangle = \sum_{\alpha_l^S,\sigma_{l+1}^S,\sigma_{l+1}^E,\alpha_l^E} \Psi^{\sigma_S\sigma_E}_{\alpha_l^S\alpha_l^E}|\alpha_l^S\rangle|\sigma_{l+1}^S\rangle|\sigma_{l+1}^E\rangle|\alpha_l^E\rangle, \tag{A11}$$

where $|\sigma_{l+1}^S\rangle$ and $|\sigma_{l+1}^E\rangle$ represent the basis of the sites added to the system and environment. The aim of the density matrix projection is to determine a subset of χ states $|\alpha_{l+1}^S\rangle$ ($|\alpha_{l+1}^E\rangle$) that optimally approximate the ground state of the enlarged system (environment) block. Accordingly, $|\alpha_{l+1}^S\rangle$ and $|\alpha_{l+1}^E\rangle$ are defined by the truncation matrices as

$$|\alpha_{l+1}^S\rangle = \sum_{\alpha_l^S} A_{\alpha_l^S\sigma_{l+1}^S,\alpha_{l+1}^S}|\alpha_l^S\rangle|\sigma_{l+1}^S\rangle, \tag{A12}$$

$$|\alpha_{l+1}^E\rangle = \sum_{\alpha_l^E} B_{\alpha_l^E\sigma_{l+1}^E,\alpha_{l+1}^E}|\alpha_l^E\rangle|\sigma_{l+1}^E\rangle, \tag{A13}$$

A and B are the isometries that realize the truncations of the basis, satisfying Eqs. (A7) and (A8) (see Fig. 15 (a) and (b)). Then the ground state with truncated basis are written as

$$|\tilde{\psi}\rangle = \sum_{\alpha_{l+1}^S\alpha_{l+1}^E} \tilde{\Psi}_{\alpha_{l+1}^S\alpha_{l+1}^E}|\alpha_{l+1}^S\rangle|\alpha_{l+1}^E\rangle. \tag{A14}$$

To minimize the truncation error that is indicated by the quadratic cost function

$$S(|\tilde{\psi}\rangle) = \| \, |\psi\rangle - |\tilde{\psi}\rangle \, \|^2, \tag{A15}$$

the truncation matrices are given by the dominant eigenvectors of the reduced density matrix

$$\rho_S = \mathrm{Tr_E}|\psi\rangle\langle\psi| = \Psi\Psi^\dagger, \tag{A16}$$

$$\rho_E = \mathrm{Tr_S}|\psi\rangle\langle\psi| = \Psi^\dagger\Psi. \tag{A17}$$

Then, with eigenvalue decomposition one can obtain A and B as

$$\rho_S = AD^2A^\dagger, \quad \rho_E = BD^2B^\dagger. \tag{A18}$$

One can easily see that A, D and B in fact give the optimal singular value decomposition (SVD) of Ψ in Eq. (A11), i.e.

$$\Psi^{\sigma_A\sigma_B}_{\alpha_l^S\alpha_l^E} \simeq \sum_{\alpha_{l+1}^S=1}^{\chi} A_{\alpha_l^S\sigma_{l+1}^S,\alpha_{l+1}^S} D_{\alpha_{l+1}^S} B_{\alpha_l^E\sigma_{l+1}^E,\alpha_{l+1}^E}, \tag{A19}$$

showing that D gives the entanglement spectrum of the ground state.

It is well-known that the ground state obtained by DMRG is actually an MPS formed by A, B and $\tilde{\Psi}$. From Fig. 15 (c), one can see that the MPS is in an orthogonal form as introduced in the previous subsection, and gives a renormalization group (RG) flow of the physical Hilbert space. The direction of the RG flow is determined by the orthogonal conditions shown in Eqs. (A7) and (A8).

3. Infinite time-evolving block decimation

In this section we will discuss of infinite time evolving block decimation, i.e. we will show how to update the iMPS for the state $|\psi\rangle$ after an application of operator $G = e^{i\hat{H}t}$:

$$|\psi(t)\rangle = e^{i\hat{H}t}|\psi(0)\rangle, \tag{A20}$$

where t can be real or imaginary. Let us assume that ψ describes an infinite translational invariant system in the form (A9), and $\hat{H}$ consists of nearest-neighbor interactions only, i.e. $\hat{H} = \sum_i h_i$, where $\hat{h}_i$ contains the interaction between sites i and $i+1$. We can then discretize time as $t = N\tau$ with $\tau \to 0$ and $N \to \infty$ and use the Trotter-Suzuki decomposition[79,80], which approximates the operator $e^{-i\hat{H}t}$. For example, the first order expansion reads:

$$e^{-i\hat{H}\tau} = e^{-i\hat{h}_1\tau}e^{-i\hat{h}_2\tau}\cdots e^{-i\hat{h}_L\tau} + O(\tau^2) \tag{A21}$$

which contains an error due to the non-commutativity of bond Hamiltonians, $[\hat{h}_i, \hat{h}_{i+1}] = 0$. The second order expansion similarly reads:

$$e^{-i\hat{H}\tau} = e^{-\frac{i}{2}\hat{H}_{\rm odd}\tau}e^{-i\hat{H}_{\rm even}\tau}e^{-\frac{i}{2}\hat{H}_{\rm odd}\tau}, \tag{A22}$$

where we have to rewrite the Hamiltonian in the following way:

$$\hat{H} = \hat{H}_{\rm odd} + \hat{H}_{\rm even} = \sum_{i\ {\rm odd}} \hat{h}_i + \sum_{i\ {\rm even}} \hat{h}_i. \tag{A23}$$

All time evolutions on odd $e^{i\hat{H}_{\rm odd}\tau}$ and even $e^{i\hat{H}_{\rm even}\tau}$ bonds respectively commute among each other, and can be carried out at the same time.

So we assume $e^{-i\hat{H}\tau}$ is specified by an infinite matrix product operator iMPO[25,26,81,82]. This iMPO is represented by a tensor $\hat{W}^{\sigma_i,\sigma_i'}_{\mu,\nu}$, where σ_i and σ_i' are physical indices and μ and ν are bond indices.

$$e^{-i\hat{H}\tau} = \hat{W}^{[1]}\hat{W}^{[2]}\cdots\hat{W}^{[l]}\cdots. \tag{A24}$$

We can find the MPO of time evolution operator, contracting an MPO for the odd bonds and the MPO for the even bonds. Now we show how to construct the MPO for the odd (even) bonds. Let us consider the Trotter step for all odd bonds of a chain:

$$e^{-i\hat{h}_1}\otimes e^{-i\hat{h}_3}\otimes\cdots e^{-i\hat{h}_{L-1}} \tag{A25}$$

It would therefore be desirable to have $O^{\sigma_1,\sigma_2,\sigma_1',\sigma_2'}$ in some form containing tensor products $O^{\sigma_1,\sigma_1'}\otimes O^{\sigma_2,\sigma_2'}$, to maintain the MPS form. At this aim we carry out a singular value decomposition:

$$O^{\sigma_1,\sigma_2,\sigma_1',\sigma_2'} = \sum_k U_k^{\sigma_1\sigma_1'}S_{k,k}V_k^{\sigma_1\sigma_1'\dagger} = \sum_k U_{1,k}^{\sigma_1\sigma_1'}U_{k,1}^{\sigma_2\sigma_2'}. \tag{A26}$$

Moreover, the MPO representing the operator in the equation (A25) is the following:

$$e^{-i\hat{H}_{\rm odd}\tau} = U^{\sigma_1\sigma_1'}U^{\sigma_2\sigma_2'}U^{\sigma_3\sigma_3'}\cdots. \tag{A27}$$

Analogously we can obtain for $e^{-i\hat{H}_{\rm even}\tau}$. Then the MPO is formed by the contraction of local tensors of MPO for the odd $e^{-i\hat{H}_{odd}}$ and even $e^{-i\hat{H}_{Even}}$ bonds (see Figs 16).

Finally the iTEBD algorithm occurs in two steps: (i) a row of tensors (which is in fact an MPO) are contracted to an MPS

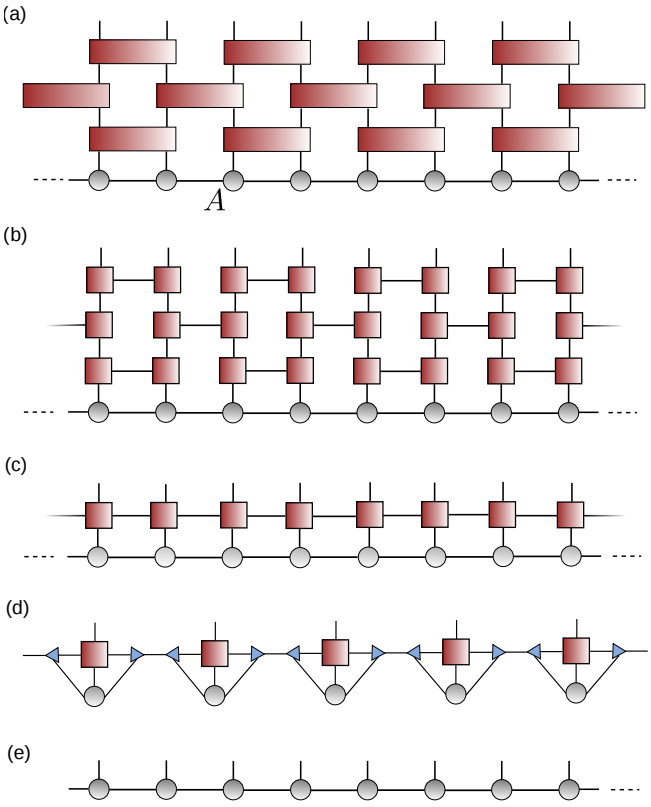

Figure 16. Graphical representation of $e^{-i\hat{H}\tau}|\psi(0)\rangle$. The operator $e^{-i\hat{H}\tau}$ is expressed in the second order Trotter decomposition.

(ii) then truncations are needed to prevent the bond dimension from being exponentially large, which are calculated by minimizing the distance between the MPS before and after truncating. While converging, the MPS is considered to be the dominant eigenvector of the MPO. In detail we have:

Contraction: The MPS we use is translational invariant, which is formed by the tensors A. In each step of iTEBD, the contraction part is given by

$$A_{s,\tilde{a}\tilde{a}'} \leftarrow \sum_{s'} T_{sbs'b'}A_{s',aa'}, \tag{A28}$$

where the new virtual bonds are entangled, satisfying $\tilde{a} = (b,a)$ and $\tilde{a}' = (b',a')$. Meanwhile, the spectrum is also updated as

$$\Lambda_{\tilde{a}} \leftarrow \Lambda_a \mathbf{1}_b, \tag{A29}$$

where $\mathbf{1}$ is a vector with $\mathbf{1}_b = 1$ for any b.

We can see that after contracting, the number of the contracted tensors is N. It means that after t iterations, the number of tensors will be reduced linearly by tN. That is the reason why we call iTBED a *linearized contraction algorithm*.

Truncation: Then, the truncation part is needed when the dimensions of the virtual bonds exceed the dimension cut-off χ. Here, we explain a simple way by local SVD to do the truncations. To truncate the virtual bond $\tilde{a}$ for example, we

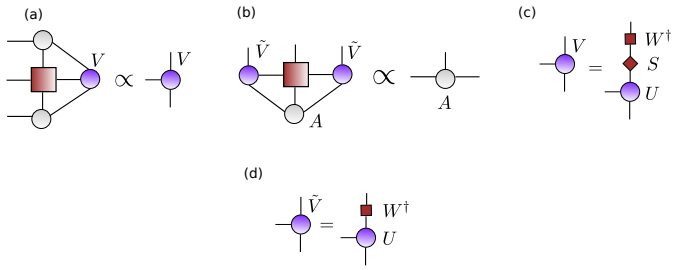

Figure 17. (Color online) The (a) and (b) show the two local eigenvalue equations given by Eqs. (A34) and (A35). The definition of $\tilde{V}$ is shown by (c) and (d).

defined a matrix by contracting the tensors connected to the target bond as

$$M_{s_1\tilde{a}_1,s_2\tilde{a}_2} = \sum_{\tilde{a}} A_{s_1,\tilde{a}_1\tilde{a}} A_{s_2,\tilde{a}\tilde{a}_2}. \tag{A30}$$

Note that it is important to have all the three spectra in the contraction.

4. Tensor network encoding

In Ref. [58], the *ab-initio* optimization principle (AOP) for the ground states of translationally invariant many-body systems was proposed based on TN. The idea is to embed the local subsystem of a unit cell in an entanglement bath that is determined self-consistently.

In the language of TN, AOP follows the idea that the contraction of an infinite TN is encoded into the contraction of the original local tensor with a proper boundary[58,83,84]. The boundary is formed by tensors called boundary tensors. In other words, boundary tensors provide the entanglement bath that optimally mimics the entanglement between the local unit cell and the rest. The boundary tensors, which can be randomly initialized, are determined by finding the fixed point of a set of local self-consistent eigenvalue equations. Then the infinite TN can be reconstructed (analogue to a "decoding" process) with the boundary tensors by utilizing the fixed-point conditions.

The central part of AOP is to solve the self-consistent eigenvalue equations that determine the boundary tensors denoted as A and V. First, one chooses a supercell, a finite block with N spins and the cell tensor T. The operator T that determines the optimization equations has defined in the following way:

$$\sum_{\{a\}} T(s,a_1,a_2)T(s,a_2,a_3)\cdots T(s,a_{N-1},a_N) = 1 - \tau\hat{H}. \tag{A31}$$

The Eq. (A31) gives the second-order Trotter-Suzuki decomposition of $e^{\tau\hat{H}}$. The tensor T can be found as suggested in[86]. Note there are many choices for a cell tensor, for example, a tensor properly formed by several cell tensors is still a cell tensor.

With the boundary tensors, two local eigenvalue equations are defined by two matrices (assumed to be Hermitian) as

$$M_{s_2b_1b_1',s_4b_2b_2'} = \sum_{s_1s_3} T_{s_1s_2s_3s_4} A^*_{s_1b_1b_2} A_{s_3b_1'b_2'}, \tag{A32}$$

$$\mathcal{H}_{s_1a_1a_2,s_3a_1'a_2'} = \sum_{s_2s_4} T_{s_1s_2s_3s_4} \tilde{V}^*_{s_2a_1a_1'} \tilde{V}_{s_4a_2a_2'}, \tag{A33}$$

where $\tilde{V}$ is obtained by the SVD of the boundary tensor V, i.e. $V = USW^\dagger$, $\tilde{V} = UW^\dagger$ (Fig. 17). The tensor $\tilde{V}$ is introduced from V in order to transform the non-local generalized eigenvalue problem to a local regular problem [Eqs (A32, A33)], where M and $\mathcal{H}$ are required to be Hermitian. The proof can be found in the Appendix in Ref.[58] and in[13]. Besides the left and right environments V of an infinite system can be calculated by projecting out the diverging extensive contributions to the Hamiltonian[87,88]. Then, the boundary tensors A and V are obtained as the dominant eigenstates of $\mathcal{H}$ and M, respectively, i.e.,

$$\sum_{s'a_2a_2'} M_{sa_1a_1',s'a_2a_2'} V_{s'a_2a_2'} \propto V_{sa_1a_1'}, \tag{A34}$$

$$\sum_{s'b_1'b_2'} \mathcal{H}_{sb_1b_2,s'b_1'b_2'} A_{s'b_1'b_2'} \propto A_{sb_1b_2}. \tag{A35}$$

In addition, the eigenvalue equation (A34) may not have a solution due to the block-triangular structure of the MPO of $\hat{H}$. This problem can be overcome quite easily for local Hamiltonians[87–89]. One can see that such two eigenvalue problems are closely related to each other: one is parametrized by the solution of the other. When the boundary tensors simultaneously solve both equations, i.e. they converge to a self-consistent fixed point, the whole infinite TN is encoded into the local contraction of the cell tensor with the boundary tensors (Fig. 18).

Specifically speaking, we start with the local contraction (a scalar) given by

$$Z = \sum T_{s_1s_2s_3s_4} V^*_{s_2a_1a_1'} V_{s_4a_2a_2'} A^*_{s_1a_1a_2} A_{s_3a_1'a_2'} \tag{A36}$$

The eigenvalue equations indicate that Z is maximized by the boundary tensors. Then, we repeatedly do the substitution with Eq. (A34) and Eq. (A35). It should be noted that the normalization of V is required here as a constraint. Then Eq. (A36) is equivalent to construct the partition function Z defined as:

$$Z = \langle\psi|\rho|\psi\rangle, \tag{A37}$$

with $|\psi\rangle$ an infinite MPS formed by the tensor A and ρ an infinite MPO formed by T.

Then, one utilizes the fact that A is the solution of the maximization of Z. It means that the MPS $|\psi\rangle$ formed by A maximizes Eq. (A37), i.e., $|\psi\rangle$ is the ground state of the MPO. In other words, we have a (non-local) eigenvalue equation

$$\rho|\psi\rangle \propto |\psi\rangle, \tag{A38}$$

under the assumption that the ground state of ρ can be effectively represented as an MPS. Eq. (A38) is true because Eq.

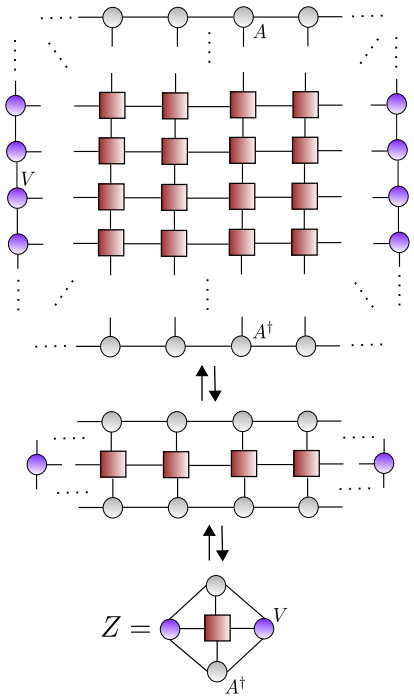

Figure 18. (Color online) The illustration of TN "encoding" (downwards) and "decoding" (upwards). One starts from an infinite TN formed by the cell tensor T with two MPSs and their conjugates defined on the boundaries along the two directions of TN. Using the eigenvalue equations (A34) and (A35), respectively, the TN contraction is firstly transformed into a 1D TN and then finally into a local contraction given by Eq. (A36). By going upwards, the infinite TN can be reconstructed from the local function, analog to a decoding process.

(A37) is maximized by $|\psi\rangle$ while one has $\langle\psi|\psi\rangle = 1$ guaranteed by the equations in Figs. 17. By substituting Eq. (A38) in Eq. (A37) repeatedly, the infinite TN formed by T can be reconstructed, meaning the whole TN is encoded into the local contraction given by Eq. (A36).

In practice, the AOP is implemented in the following steps:

- **Step 1:** From the Hamiltonian $\hat{H}$ define the local tensor T.
- **Step 2:** Give an initial guess of the tensor A. While its elements can be totally random, it is better to make the two ancillary indexes symmetrical so that M could be Hermitian.
- **Step 3:** Calculate M and its dominant eigenstate V which is actually a third-order tensor. To compute this eigenvalue problem, one can use V obtained from the last iteration as the initial guess.
- **Step 4:** Calculate $\tilde{V}$ from V, and the effective Hamiltonian $\mathcal{H}$; solve its eigenstate A. Again, one can use the A obtained in the last iteration as the initial guess.
- **Step 5:** Check if A converges. If it does, proceed to Step 6; if not, go back to Step 3.
- **Step 6:** Use the tensor A to construct the spatial MPS and $|V\rangle$ for the tMPS; calculate the interested physical quantities.

We shall remark several important differences comparing AOP with the existing schemes:

(1) In iDMRG[16,17,25,26], one usually uses the MPO of Hamiltonian $\hat{H}$ to construct the effective Hamiltonian. In this case, the dynamic correlation length as well as the excitation gap could not be obtained from the tMPS.

(2) In iTEBD[37], one can still define the tMPS by the truncation matrices, as argued in Ref.[58] and above, but there are some complexities from the freedom of choosing the truncations. In this case, canonicalization[40] should be necessary and the stability is to be explored.

(3) In the CTM algorithm, the strategy is to break up the infinite tensor network in different regions with a fixed dimensions and we can find an effective corner environment by solving a fixed point equation. In particular in CTM algorithm we define the fixed point equation on the corner transfer matrix. This implies that asymptotically the fixed point can be well approximated by an MPS.

(4) The tMPS is similar to the transverse contraction algorithm with the folding trick[60], but these two schemes have completely different alms and advantages. In the former, the transverse contraction is the optimal way to compute the real-time evolution where there is much less entanglement to capture. In our scheme, the tMPS is more treated as a physical state that reveals the properties of the quantum system. Algorithmically, it is similar to the transfer-matrix renormalization group for thermal states[19,20], when applied to calculating ground states. In these schemes, the translational invariance in the time direction is not explicit and it is not easy to define an effective Hamiltonian that gives the dynamic correlation length.

5. Calculations of correlation length

In the following, we explain how the correlation length of an translationally invariant MPS is calculated from the eigenvalues of the transfer matrix. This trick has been used frequently.

Let us explain with TN the calculation of $\mathcal{C}(d\beta) = \langle\hat{S}_{\beta_1}\hat{S}_{\beta_2}\rangle$ with $d\beta = \beta_2 - \beta_1$ ($\beta_1 < \beta_2$), where the two spin operators are put in the same site but at different imaginary time β_1 and β_2. Fig. 2 gives its TN representation (up to a normalization factor). From the argument with iTEBD, we know that the tMPS is the dominant eigenstate of the MPO defined by an infinite stripe of the TN in the vertical direction, thus, $\langle\hat{S}_{\beta_1}\hat{S}_{\beta_2}\rangle$ can be simplified as the contraction of the tMPSs with one vertical stripe of the TN (right side of Fig. 2).

Now it is clear to see that $\langle\hat{S}_{\beta_1}\hat{S}_{\beta_2}\rangle$ is the matrix product of infinite $\mathcal{H}$'s and two spin operators: there are $K = (\beta_2 - \beta_1)/\tau$ of $\mathcal{H}$'s between these two operators with infinite $\mathcal{H}$'s on both sides. It means that the decay of $\mathcal{C}(d\beta)$ is dominated by the gap between the first and second eigenvalues (denoted

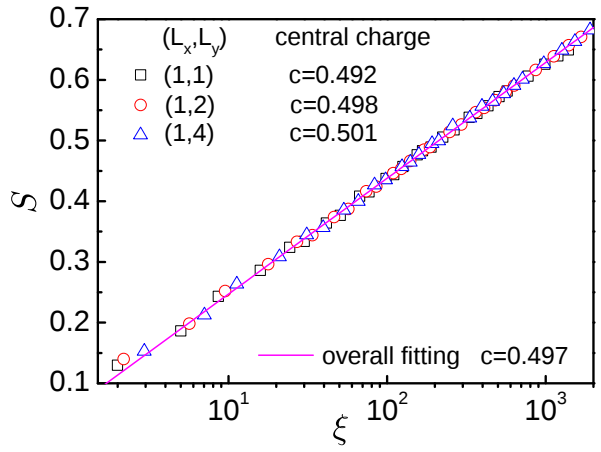

Figure 19. (Color online) The entanglement entropy S against correlation length ξ of the tMPS in 2D Ising model at the critical temperature is given. By varying the dimension cut-off $\chi = 2 \sim 50$ and the cell tensor of size (L_x, L_y), an intrinsic logarithmic scaling behavior is observed, which is independent of calculation parameters. The central charge c from the fitting with different (L_x, L_y) is accurately obtained (with the exact solution $c = 0.5$). The results from the spatial MPS are the same as those from the tMPS with the difference $\sim O(10^{-5})$.

by η_0 and η_1) of $\mathcal{H}$, i.e.,

$$\mathcal{C}(d\beta) \propto [\frac{\eta_1}{\eta_0}]^K. \tag{A39}$$

Here we take into account the fact that at the quantum critical point, $\langle \hat{S} \rangle$ still vanishes, thus $\mathcal{C}(\infty) = 0$. Then, one can readily obtain the dynamic correlation length

$$\tilde{\xi}_T = \frac{1}{\tilde{\Delta}}, \tag{A40}$$

with $\tilde{\Delta} = \ln \eta_0 - \ln \eta_1$ the logarithmic gap of $\mathcal{H}$ and $\tilde{\xi}_T = \xi_T \tau$ where ξ_T is the correlation length calculated directly to the tMPS. The dynamic correlation function is known to possess a linear relation with the inverse of the system gap Δ[1], satisfying $\tilde{\xi}_T \propto 1/\Delta$. Then, we have the simple relation between the logarithmic gap of $\mathcal{H}$ and the gap of the model as

$$\Delta \propto \tilde{\Delta}. \tag{A41}$$

Appendix B: Two-dimensional classical Ising partition function

In this section, we apply the TN encoding scheme to 2D classical Ising model at the criticality. There are some intrinsic differences between their TN representations. For the 2D classical partitioning, the two dimensions of the TN are both spatial and discrete, and they are equivalent to each other.

Its partition function can be directly written in a 2D TN, where the local tensor is the probability distribution of some local Ising spins. Here, we take the Ising model on square lattice as an example, where the local tensor is defined as

$$T_{s_1 s_2 s_3 s_4} = e^{-\beta(s_1 s_2 + s_2 s_3 + s_3 s_4 + s_4 s_1)}, \tag{B1}$$

with β the inverse temperature and the spin index $s_i = \pm 1$. Note that the local tensor of the TN can also be chosen as the contraction of several T's.

It is well-known that the dominant eigenstate of the transfer matrix can be approximated as an MPS. Each MPS with a finite bond dimension χ corresponds to a gapped state with a finite correlation length ξ and entanglement entropy S. At the critical temperature, the central charge can be extracted by the scaling behavior of S against ξ[64–66]. Specifically speaking, with different χ, ξ and S satisfy

$$S = \frac{c}{6} \ln \xi + const, \tag{B2}$$

where the coefficient gives the central charge c. Note that Eq. (B2) is independent of calculation parameters. Meanwhile, one can also check the scaling behavior with different χ's separately and have

$$\xi \propto \chi^{\kappa}, \tag{B3}$$

$$S = \frac{c\kappa}{6} \ln \chi + const. \tag{B4}$$

By substituting, one can readily have Eq. (B2) from these two equations. For the 2D Ising model, we have the critical temperature $\beta_c = \ln(1+\sqrt{2})/2$ from the exact solution[85] and $c = 1/2$ that corresponds to a free fermionic field theory[64]. We shall stress that for any finite χ, we cannot exactly give a critical state by MPS, but only a gapped. The central idea of the scaling theory with MPS is to extract the conformal data from the scaling behaviors the gapped MPSs.

In Fig. 19, we show that the MPS from iDMRG has the same correlation length ξ and entanglement entropy S as the vertical MPS obtained simultaneously in the iTEBD in the other direction with the difference $O(10^{-5})$. In other words, these two MPSs, though updated within two different schemes and located in two different directions of the TN, are connected by a gauge transformation. By choosing different bond dimension cut-offs and cells to construct the tensor T, the relation between ξ and S shows a robust logarithmic scaling, giving accurately the central charge. The precision increases with the size of the cell tensor L_x and L_y.

* Corresponding author. Email: shi-ju.ran@icfo.eu

[1] S. Sachdev, *Quantum Phase Transitions, 2nd ed.* Cambridge University Press, Cambridge, (2011).
[2] C. Lacroix, P. Mendels, and F. Mila, *Introduction to frustrated Magnetism*, Springer, Heidelberg, (2011).
[3] M. Lewenstein, A. Sanpera, and V. Ahufinger, *Ultracold atoms in optical lattices: Simulating quantum many-body systems*, Oxford University Press (2012).
[4] C. Castelnovo, R. Moessner, and S. Sondhi, *Spin Ice, Fractionalization, and Topological Order*, Ann. Rev. Cond. Mat. Phys. **3**, 35

(2012).

[5] P. W. Anderson, *The Resonating Valence Bond State in La_2CuO_4 and Superconductivity*, Science **235**, 1196 (1987).

[6] P. A. Lee, N. Nagaosa and X. G. Wen, *Doping a Mott insulator: Physics of high-temperature superconductivity*, Rev. Mod. Phys. **78**, 17 (2006).

[7] J. M. Kosterlitz and J. Thouless, *Long range order and metastability in two dimensional solids and superfluids (Application of dislocation theory)*, Solid State Phys. **5**, L124 (1972).

[8] B. A. Bernevig and T. L. Hughes, *Topological Insulators and Topological Superconductors*, Princeton University Press (2013).

[9] L. Balents, *Spin liquids in frustrated magnets*, Nature **464**, 199-208 (2010).

[10] A. Banerjee, C. A. Bridges, J. Q. Yan, A. A. Aczel, L. Li, M. B. Stone, G. E. Granroth, M. D. Lumsden, Y. Yiu, J. Knolle, S. Bhattacharjee, D. L. Kovrizhin, R. Moessner, D. A. Tennant, D. G. Mandrus, and S. E. Nagler, *Proximate Kitaev quantum spin liquid behaviour in a honeycomb magnet*, Nat. Mat. doi:10.1038/nmat4604 (2016).

[11] R. Orús, *A Practical Introduction to Tensor Networks: Matrix Product States and Projected Entangled Pair States*, Ann. Phys. **349**, 117 (2014).

[12] U. Schollwök, *The density-matrix renormalization group in the age of matrix product states*, Ann. Phys. **96**, 326 (2011).

[13] S-J. Ran, E. Tirrito, C. Peng, X. Chen, G. Su and M. Lewenstein, *Review of tensor network contraction approaches*, arXiv:1708.09213.

[14] F. Verstraete, V. Murg, and J. I. Cirac, *Matrix product states, projected entangled pair states, and variational renormalization group methods for quantum spin systems*, Adv. Phys. **57**, 143 (2008).

[15] J. Eisert, M. Cramer, and M. B. Plenio, *Area laws for the entanglement entropy a review*, Rev. Mod. Phys **20**, 30 (2009).

[16] S. R. White, *Density matrix formulation for quantum renormalization groups*, Phys. Rev. Lett. **69**, 2863 (1992).

[17] S. R. White, *Density-matrix algorithms for quantum renormalization groups*, Phys. Rev. B **48**, 10345 (1993).

[18] K. G. Wilson, *The renormalization group: Critical phenomena and the Kondo problem*, Rev. Mod. Phys. **47**, 773 (1975).

[19] R. J. Bursill, T. Xiang, and G. A. Gehring, *The density matrix renormalization group for a quantum spin chain at non-zero temperature*, J. Phys. Cond. Matter **8**, L583 (1996).

[20] X. Q. Wang and T. Xiang, *Transfer-matrix density-matrix renormalization-group theory for thermodynamics of one-dimensional quantum systems*, Phys. Rev. B **56**, 5061 (1997).

[21] A. E. Feiguin and S. R. White, *Finite-temperature density matrix renormalization using an enlarged Hilbert space*, Phys. Rev. B **72**, 220401(R) (2005).

[22] E. M. Stoudenmire and S. R. White, *Studying Two-Dimensional Systems with the Density Matrix Renormalization Group.*, Ann. Rev. Cond. Matter Phys. **3**, 111 (2012).

[23] G. K.-L. Chan, A. Keselman, N. Nakatani, Z. D. Li, and S. R. White, *Matrix Product Operators, Matrix Product States, and ab initio Density Matrix Renormalization Group algorithms*, The Journal of chemical physics **145**, 014102 (2016).

[24] S. Östlund and S. Rommer, *Thermodynamic Limit of Density Matrix Renormalization*, Phys. Rev. Lett. **75**, 3537 (1995).

[25] I. P. McCulloch, *From density-matrix renormalization group to matrix product states.*, J. Stat. Mech. **2007**, P10014 (2007).

[26] I. P. McCulloch, *Infinite size density matrix renormalization group*, arXiv:0804.2509 .

[27] E. Tirrito, S.-J. Ran, A. J. Ferris and M. Lewenstein, *An efficient perturbation theory of density matrix renormalization group*, Phys. Rev. B **95**, 064110 (2017).

[28] F. Verstraete and J. I. Cirac, *Continuous Matrix Product States for Quantum Fields*, Phys. Rev. Lett. **104**, 190405 (2010).

[29] M. B. Hastings and R. Mahajan, *Connecting entanglement in time and space: Improving the folding algorithm*, Phys. Rev. A **91**, 032306 (2015).

[30] V. Stojevic, J. Haegeman, I. P. McCulloch, L. Tagliacozzo, and F. Verstraete, *Conformal data from finite entanglement scaling*, Phys. Rev. B **91**, 035120 (2015).

[31] S. S. Chung, K. Sun, and C. J. Bolech, *Matrix product ansatz for Fermi fields in one dimension*, Phys. Rev. B **91**, 121108(R) (2015).

[32] M. Fannes, B. Nachtergaele, and R. F. Werner, *Exact Antiferromagnetic Ground States of Quantum Spin Chains*, Europhys. Lett. **10**, 633 (1989).

[33] M. Fannes, B. Nachtergaele, and R. F. Werner, *Finitely correlated states on quantum spin chains*, Comm. Math. Phys. **144**, 443 (1992).

[34] M. M. Rams, V. Zauner, M. Bal, J. Haegeman, and F. Verstraete, *Truncating an exact matrix product state for the XY model: Transfer matrix and its renormalization*, Phys. Rev. B **92**, 235150 (2015).

[35] G. Vidal, *Efficient Classical Simulation of Slightly Entangled Quantum Computations*, Phys. Rev. Lett. **91**, 147902 (2003).

[36] G. Vidal, *Efficient Simulation of One-Dimensional Quantum Many-Body Systems*, Phys. Rev. Lett. **93**, 040502 (2004).

[37] G. Vidal, *Classical Simulation of Infinite-Size Quantum Lattice Systems in One Spatial Dimension*, Phys. Rev. Lett. **98**, 070201 (2007).

[38] M. Suzuki and M. Inoue, *The ST-Transformation Approach to Analytic Solutions of Quantum Systems. I General Formulations and Basic Limit Theorems*, Prog. Theor. Phys. **78**, 787-799 (1987).

[39] M. Inoue and M. Suzuki, *The ST-Transformation Approach to Analytic Solutions of Quantum Systems. II Transfer-Matrix and Pfaffian Methods*, Prog. Theor. Phys. **79**, 645 (1998).

[40] R. Orús and G. Vidal, *Infinite time-evolving block decimation algorithm beyond unitary evolution*, Phys. Rev. B **78**, 155117 (2008).

[41] M. Levin and C. P. Nave, *Tensor Renormalization Group Approach to Two-Dimensional Classical Lattice Models*, Phys. Rev. Lett. **99**, 120601 (2007).

[42] H. C. Jiang, Z. Y. Weng, and T. Xiang, *Accurate Determination of Tensor Network State of Quantum Lattice Models in Two Dimensions*, Phys. Rev. Lett. **101**, 090603 (2008).

[43] Z. C. Gu, M. Levin, and X. G. Wen, *Tensor-entanglement renormalization group approach as a unified method for symmetry breaking and topological phase transitions*, Phys. Rev. B **78**, 205116 (2008).

[44] Z. C. Gu and X. G. Wen, *Tensor-entanglement-filtering renormalization approach and symmetry-protected topological order*, Phys. Rev. B **80**, 155131 (2009).

[45] L. Wang and F. Verstraete, *Cluster update for tensor network states*, arXiv:1110.4362.

[46] W. Li, J. von Delft, and T. Xiang, *Efficient simulation of infinite tree tensor network states on the Bethe lattice*, Phys. Rev. B **86**, 195137 (2012).

[47] P. Czarnik, L. Cincio, and J. Dziarmaga, *Projected entangled pair states at finite temperature: Imaginary time evolution with ancillas*, Phys. Rev. B **86**, 245101 (2012).

[48] P. Czarnik and J. Dziarmaga, *Projected Entangled Pair States at Finite Temperature: Iterative Self-Consistent Bond Renormalization for Exact Imaginary Time Evolution*, Phys. Rev. B **92**, 035120 (2015).

[49] Z. Y. Xie, J. Chen, M. P. Qin, J. W. Zhu, L. P. Yang, and T. Xiang, *Coarse-graining renormalization by higher-order singular value decomposition*, Phys. Rev. B **86**, 045139 (2012).

[50] J. Jordan, R. Orús, G. Vidal, F. Verstraete, and J. I. Cirac, *Classical Simulation of Infinite-Size Quantum Lattice Systems in Two Spatial Dimensions*, Phys. Rev. Lett. **101**, 250602 (2008).

[51] Z. Y. Xie, H. C. Jiang, Q. N. Chen, Z. Y. Weng, and T. Xiang, *Second Renormalization of Tensor-Network States*, Phys. Rev. Lett. **103**, 160601 (2009).

[52] H. N. Phien, J. A. Bengua, H. D. Tuan, P. Corboz, and R. Orús, *Infinite projected entangled pair states algorithm improved: Fast full update and gauge fixing*, Phys. Rev. B **92** 035142 (2015).

[53] R. J. Baxter, *Dimers on a rectangular lattice*, J. Math. Phys. **9** 650 (1968).

[54] R. J. Baxter, *Variational approximations for square lattice models in statistical mechanics*, J. Stat. Phys., **19**, 461 (1978).

[55] T. Nishino and K. Okunishi, *Corner transfer matrix renormalization group method*, J. Phys. Soc. Jpn. 65, 891 (1996).

[56] R. Orús and G. Vidal, *Simulation of two-dimensional quantum systems on an infinite lattice revisited: Corner transfer matrix for tensor contraction*, Phys. Rev. B **80**, 094403 (2009).

[57] R. Orús, *Exploring corner transfer matrices and corner tensors for the classical simulation of quantum lattice systems*, Phys. Rev. B **85**, 205117 (2011).

[58] S. J. Ran, *Ab initio optimization principle for the ground states of translationally invariant strongly correlated quantum lattice models*, Phys. Rev. E **93** 053310 (2016).

[59] S. J. Ran, A. Piga, C. Peng, G. Su, and M. Lewenstein, *Few-body systems capture many-body physics: tensor network approach*, Phys. Rev. B **96** 155120 (2017).

[60] M. C. Bañuls, M. B. Hastings, F. Verstraete, and J. I. Cirac, *Matrix Product States for Dynamical Simulation of Infinite Chains*, Phys. Rev. Lett. **102**, 240603 (2009).

[61] P. Pfeuty, *The one-dimensional Ising model with a transverse field*, Ann. Phys. **57**, 79-90 (1970).

[62] H. Katsura, and I. Maruyama, *Derivation of the matrix product ansatz for the Heisenberg chain from the algebraic Bethe ansatz*, Journal of Physics A: Mathematical and Theoretical **43**, 175003 (2010).

[63] I. Maruyama, and H. Katsura, *Continuous matrix product ansatz for the one-dimensional Bose gas with point interaction*, Journal of the Physical Society of Japan **79**, 073002 (2010).

[64] G. Vidal, J. I. Latorre, E. Rico, and A. Kitaev, *Entanglement in quantum critical phenomena*, Phys. Rev. Lett. **90**, 227902 (2003).

[65] L. Tagliacozzo, T. R. de Oliveira, S. Iblisdir, and J. I. Latorre, *Scaling of entanglement support for matrix product states*, Phys. Rev. B **78**, 024410 (2008).

[66] F. Pollmann, S. Mukerjee, A. M. Turner, and J. E. Moore, *Theory of Finite-Entanglement Scaling at One-Dimensional Quantum Critical Points*, Phys. Rev. Lett. **102**, 255701 (2009).

[67] V. Stojevic, J. Haegeman, I. P. McCulloch, L. Tagliacozzo, and F. Verstraete, *Conformal data from finite entanglement scaling*, Phys. Rev. B **91**, 035120 (2015).

[68] B. Pirvu, G. Vidal, F. Verstraete, and L. Tagliacozzo, *Matrix product states for critical spin chains: finite size scaling versus finite entanglement scaling*, Phys. Rev. B **86**, 075117 (2012).

[69] J. B. Kogut, *An introduction to lattice gauge theory and spin systems*, Rev. Mod. Phys. **51**, 659 (1979).

[70] J. L. Cardy, *Operator content of two-dimensional conformally invariant theories*, Nuclear Phys. B **270**, 186204 (1986).

[71] J. L. Cardy, *Effect of boundary conditions on the operator content of two-dimensional conformally invariant theories*, Nucl. Phys. B **275**, 200218 (1986).

[72] M. Henkel, *Finite-size scaling and universality in the spectrum of the quantum ising chain. I. Periodic and antiperiodic boundary condition*, J. Phys. A: Mathematical and General **20**, 9951010 (1987).

[73] G. Evenbly, R. N. C. Pfeifer, V. Pico, S. Iblisdir, L. Tagliacozzo, I. P. McCulloch, and G. Vidal *Boundary quantum critical phenomena with entanglement renormalization*, Physical Review B **82**, 161107 (2010).

[74] A. B. Zamolodchikov, *Integrals Of Motion and S-Matrix of the (scaled) T = Tc Ising Model with magnetic field*, Int. J. Mod. Phys. A **4**, 4235 (1989).

[75] M. Henkel and H. Saleur, *The two-dimensional Ising model in the magnetic field: a numerical check of Zamolodchikovs conjecture*, J. Phys. A Mathematical and General **22**, L513L518 (1989).

[76] G. Delfino, G. Mussardo, and P. Simonetti *Non-integrable Quantum Field Theories as Perturbations of Certain Integrable Models*, Nucl. Phys. B **473**:469-508,(1996).

[77] G. Delfino, P. Grinza, and G. Mussardo *Decay of particles above threshold in the Ising field theory with magnetic field*, Nucl.Phys. B**737** (2006) 291-303.

[78] A. J. Daley, C. Kollath, U. Schollwöck, and G. Vidal, *Time-dependent density-matrix renormalization-group using adaptive effective Hilbert spaces*, J. Stat. Mech.: Theor. Exp., P04005 (2004).

[79] M. Suzuki, *Fractal decomposition of exponential operators with applications to many-body theories and Monte Carlo simulations*, Phys. Lett. A **146**, 319 (1990).

[80] M. Suzuki, *General theory of fractal path integrals with applications to many-body theories and statistical physics*, J. Math. Phys. **32**, 400 (1991).

[81] G. M. Crosswhite, A. C. Doherty, and G. Vidal, *Applying matrix product operators to model systems with long-range interactions*, Phys. Rev. B **78**, 035116 (2008).

[82] V. Nebendahl and W. Dür, *Improved numerical methods for infinite spin chains with long-range interactions*, Phys. Rev. B **87**, 075413 (2013).

[83] S. J. Ran, W. Li, B. Xi, Z. Zhang, and G. Su, *Optimized Decimation of Tensor Networks with Super-orthogonalization for Two-Dimensional Quantum Lattice Models*, Phys. Rev. B **86**, 134429 (2012).

[84] S. J. Ran, B. Xi, T. Liu, and G. Su, *Theory of Network Contractor Dynamics for Exploring Thermodynamic Properties of Two-dimensional Quantum Lattice Models*, Phys. Rev. B **88**, 064407 (2013).

[85] L. Onsager, *Crystal Statistics. I. A Two-Dimensional Model with an Order-Disorder Transition*, Phys. Rev. **65**, 117 (1944).

[86] M. P. Zaletel, R. S. K. Mong, C. Karrasch, J. E. Moore, and F. Pollmann, *Time-evolving a matrix product state with long-ranged interactions* , Phys. Rev. B, **91**, 165112 (2015).

[87] J. Haegeman, J. I. Cirac, T. J. Osborne, I. Pizorn, H. Verschelde, and F. Verstraete, *Time-dependent variational principle for quantum lattices*, Phys. Rev. Lett., **107**(7), 070601 (2011).

[88] M. Ganahl, J. Rincón, and G. Vidal, *Continuous Matrix Product States for Quantum Fields: An Energy Minimization Algorithm*, Phys. Rev. Lett., **118**(22), 220402 (2017).

[89] M. L. Wall and Lincoln D. Carr, *Out of equilibrium dynamics with Matrix Product States*, New J. Phys., **14** 125015 (2012)

[90] J. Haegeman, C. Lubich, I. Oseledets, B. Vandereycken, and F. Verstraete, *Unifying time evolution and optimization with matrix product states*, Phys. Rev. B **94**, 165116 (2016).